Low temperature dependence of resistivity in obliquely sputter-deposited gold thin films

Nicolas Martin[1, *], Eliot Martin[2], Jean-Marc Cote[1], Fabrice Sthal[1], Joseph Gavoille[1], Marina Raschetti[3], and Stefania Oliveri[3]

[1] SUPMICROTECH, CNRS, Institut FEMTO-ST, F-25000 Besançon Cedex, France

[2] Ecole Normale Supérieure Paris-Saclay, 4, Avenue des Sciences 91190 Gif-sur-Yvette, France

[3] Université de Franche-Comté, CNRS, Institut FEMTO-ST, F-25000 Besançon Cedex, France

* Corresponding author: nicolas.martin@femto-st.fr

Highlights

- Au thin films are sputtered by oblique angle deposition with an angle $\alpha = 0°$ to 80°.

- A porous and tilted columnar architecture is produced for glancing deposition angles.

- Resistivity *vs.* temperature is used to assess electron-phonon interactions.

- The electron-phonon coupling strength enhances for high deposition angles.

Graphical abstract

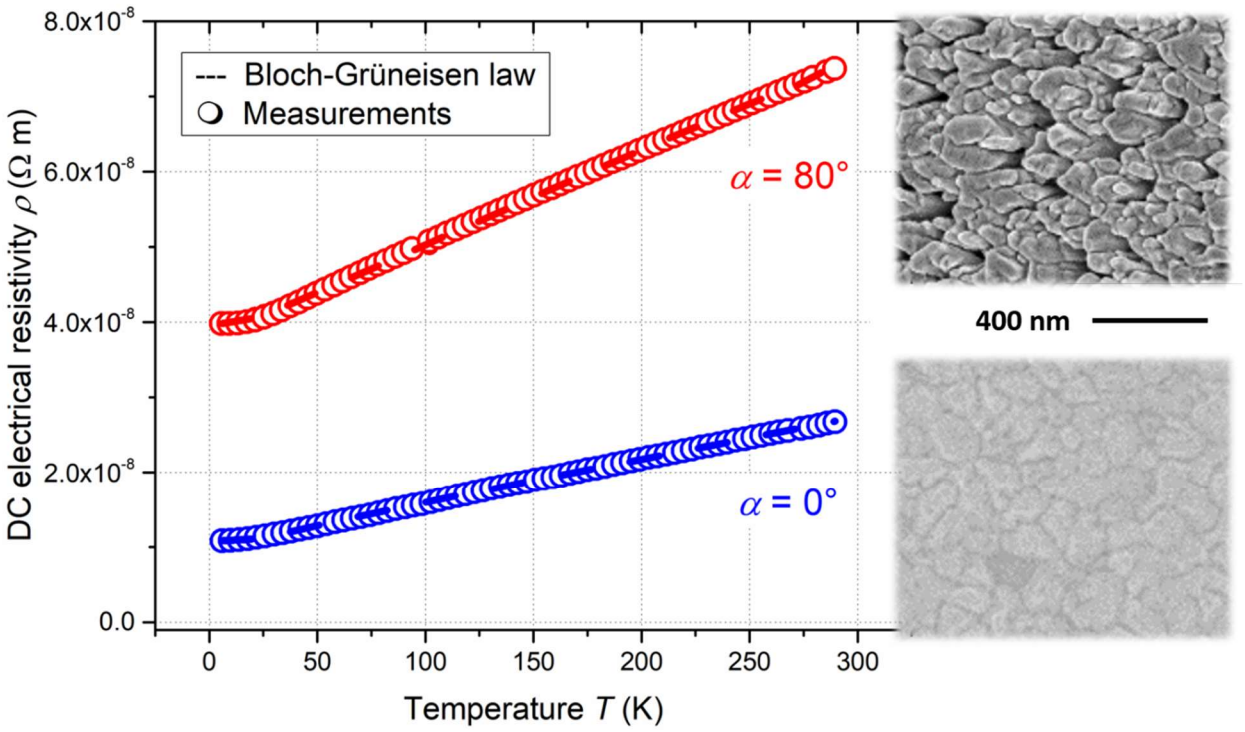

Abstract

We report on the electrical resistivity at low temperature of Au thin films 400 nm thick deposited by DC magnetron sputtering using oblique angle deposition (OAD). The deposition angle α is gradually and systematically changed from 0° to 80°. A tilted and voided columnar structure is produced for deposition angles higher than 60°, whereas the lowest angles lead to a dense and compact structure with no clear cross-section morphology. Resistivity *vs.* temperature measurements reveal a typical metallic-like behavior in the range 7–300 K whatever the deposition angle. The latter gives rise to a significant increase of residual resistivity and temperature coefficient of resistance, and again for the most grazing angles, *i.e.*, $\alpha > 60°$. The Bloch-Grüneisen model is assumed for understanding the evolution of electron-phonon interactions as a function of the deposition angle. This enhanced resistivity is connected to the structural defects and the porous architecture especially emphasized for glancing angles, and the strengthening of the electron-phonon coupling for high deposition angles.

Keywords: Gold, Thin films, Oblique angle deposition, Resistivity, Electron-phonon interaction.

1. Introduction

The in-depth understanding of electronic transport mechanisms in elementary metals still remains a scientific challenge, especially at very low temperature since the electron scattering in solid state materials strongly depends on various types of interactions with defects, impurities, grain boundaries, phonons and so on [1, 2]. These different electron scattering phenomena can be more or less relevant as the temperature changes and for a given range of temperatures, but particularly according to the geometry and dimension of the system (wires, thin films or bulk materials) [3-5]. Electron scattering can be strongly disturbed in thin films exhibiting structural variations at the nano- and micrometric scales. Although electron mean free path commonly appears as a key parameter for the electrical conductivity of metallic films, the electronic transport properties can also be influenced by structural parameters such as the atomic long-range order, the material roughness or its structure [6, 7]. When the temperature changes, many transport properties of metals and especially electrical resistivity become temperature dependent and interactions of electrons with 1D, 2D or 3D defects and phonons have to be assumed.

The electrical resistivity *vs.* temperature of metallic thin films classically exhibits a linear behavior due to the coupling between free electrons and lattice vibrations. When the temperature is well below the Debye temperature, namely θ_D, of the bulk metal (*i.e.*, for temperatures lower than around $\theta_D/10$), the electron-defects scattering mechanism prevails which leads to the residual resistivity; the latter being related to the purity and crystalline order of the as-deposited metal [8]. Both of these electrical resistivity *vs.* temperature characteristics can be largely influenced by the structural properties of the film, and consequently by the film growth. About 30 years ago, oblique angle deposition (OAD) process appeared as an original approach for easily and successfully tuning the film architecture (tilted columns, zigzags, helices and so on) and thus, a relevant strategy to play with the size effect at various scales [9-11]. For the last decades, many studies have been published about the resistivity at room temperature of OAD films and how it can be affected by the deposition

angle [12-15]. The resistivity behavior of a large number of materials has ever been studied, including several metals [16-18]. It is worth noting that the deposition angle dependence is very similar for each material, *i.e.*, a strong increase of resistivity when deposition angle α is higher than around 60°, with a variation of 2 to 3 orders of magnitude over the full α range (0° to 80° for instance). This sudden increase of resistivity is mainly assigned to structural changes induced by the shadowing effect at the atomic scale during the film growth [19]. OAD films is commonly assumed as a disordered mixture of conducting (material) and insulating (voids and oxides) media. Preparing films at high deposition angles increases the void fraction in the film, which reduces the conductive paths of charge carriers and thus favoring the resistive behavior. While many investigations have ever been devoted to the room temperature resistivity of AOD films, a few researches have been focused at high temperatures [20-22]. Through an annealing treatment in air, some authors studied the effect of a rising temperature on electrical resistivity of metallic OAD films, clearly showing an oxidation phenomenon, especially for the highest deposition angles [23, 24]. Only a few studies reports on the very low temperature dependence of OAD films [25, 26]. As a result, this kind of study remains a scientific motivation, particularly for understanding electron scattering mechanisms related to lattice vibrations, structural disorders and defects, which are especially significant in OAD films.

In this study, we report on electronic transport properties of tilted columnar gold thin films sputter-deposited by OAD by means of a systematic change of the deposition angle α from 0° to 80°. Gold material has been chosen since OAD films are very sensitive to oxidation especially at high deposition angle (number of voids increases giving rise to a mixture of metallic and oxide phases). As a result, implementation of gold allows correlating some variations of properties with micro- and nanostructure, preventing some effects related to the film composition. DC electrical resistivity *vs.* temperature is systematically measured in the temperature range 7-300 K. Structural analyses are also performed and, electron-phonon as well as electron-defect interactions are particularly discussed based-on the Bloch-Grüneisen theory.

2. Material and methods

Au thin films were prepared on glass and (100) silicon substrates from a pure gold metallic target (99.9 at.% of purity and 51 mm diameter) in a homemade DC magnetron sputtering system. Briefly, the system was a 40 L vacuum chamber. It was evacuated with pumping units (turbomolecular pump backed with a primary pump) leading to a residual pressure lower than 10^{-5} Pa. The distance between the center of the substrate and that of the target was 65 mm. The gold target was sputtered in a pure argon atmosphere with a flow rate of 2.6 sccm. A constant pumping speed of 13 L s^{-1} was used giving rise to an argon sputtering pressure of 0.3 Pa. The target current was fixed at 200 mA for all depositions. Substrates (glass and (100) Si) were grounded during all depositions with no external heating. They were ultrasonically cleaned in acetone and ethanol before thin films deposition. The deposition angle α was progressively changed using the following angles: 0, 30, 60, 70 and 80°. The deposition time was adjusted to get the same film thickness (obtained by profilometry) of 400 nm for each deposition angle.

Microstructural characterization was performed on Au thin films deposited on silicon substrates. The morphology was investigated using a scanning electron microscope (SEM) Helios Nanolab 600i (FEI) to view the top and cross-section of the films. The crystallographic structure was studied by X-ray diffraction (XRD) technique. Patterns were recorded using a PAnalytical Aeris diffractometer with a copper X-ray source (Cu $\lambda_{K\alpha1,2}$ = 0.15418 nm) following the grazing incidence configuration (GIXRD). An incidence angle θ = 0.8° was used and scans were performed with 2θ angle from 20° to 90° with a step of 0.02° per 1 s. DC electrical resistivity measurements were carried out from 7 to 300 K for Au thin films deposited on glass substrates using the four-probe van der Pauw method. A cryostat system from Advanced Research Systems Incorporation (ARS cryocooler series CS-204-AE) was used to cool the sample temperature down to about 6 K in a chamber equipped with

a pumping system leading to a vacuum below 10^{-4} Pa. A temperature ramp of 1 K min^{-1} was systematically applied for all resistivity measurements.

3. Results and discussion

3.1 Structure and morphology

Deposition rate of Au films exhibits a typical decrease as a function of deposition angle. It can be normalized dividing the experimental growth rate measured at any deposition angle by those obtained at normal incidence ($\alpha = 0°$). This defines a normalized growth rate (*NGR*), which can be fitted according to the following equation (1) proposed by Poxson *et al.* [27]:

$$NGR = \frac{\cos\alpha}{1 - \frac{\alpha \tan\alpha}{c + \tan\alpha}} \quad (1)$$

Where

NGR is the normalized growth rate (arb. units), α the deposition angle (°) and *c* is a fitting parameter defined by:

$$c = \frac{\pi V_{material}}{2 A_{cs} h} \quad (2)$$

With

$V_{material}$ is the volume of the deposited material, *i.e.*, volume of one nanocolumn (m^3), A_{cs} the cross-sectional area due to the shadowing created by the nanocolumn (m^2) and *h* the height of the nanocolumn (m). Fig. 1 shows a good agreement between experimental deposition rates and Poxson's equation using $c = 6.47$. It is worth of noting a gradual decrease of *NGR vs.* α with a rate around 40% of the conventional one ($\alpha = 0°$) when the deposition angle reaches 80°. Extrapolating at $\alpha = 90°$ does not lead to a null rate, which well agrees with former studies reporting a very tilted columnar films on vertical walls of substrates [28] or when OAD is performed with a deposition angle tending to 90° [29]. This substantial growth rate produced by sputtering with $\alpha = 90°$ is assigned to the dispersion of sputtered particles by the gaseous atmosphere. Since the argon sputtering pressure was

0.3 Pa, the mean free path of Au atoms is 53 mm [30]. In addition, calculation of the thermalization degree [31] leads to a significant part of thermalized Au atoms with 42% for a deposition angle α = 80° and so 52% of ballistic Au atoms. As a result, increasing the deposition angle favors impingement of dispersed particles on the film and so, the growth of gold material even on surfaces, which are sheltered from the incoming sputtered flux.

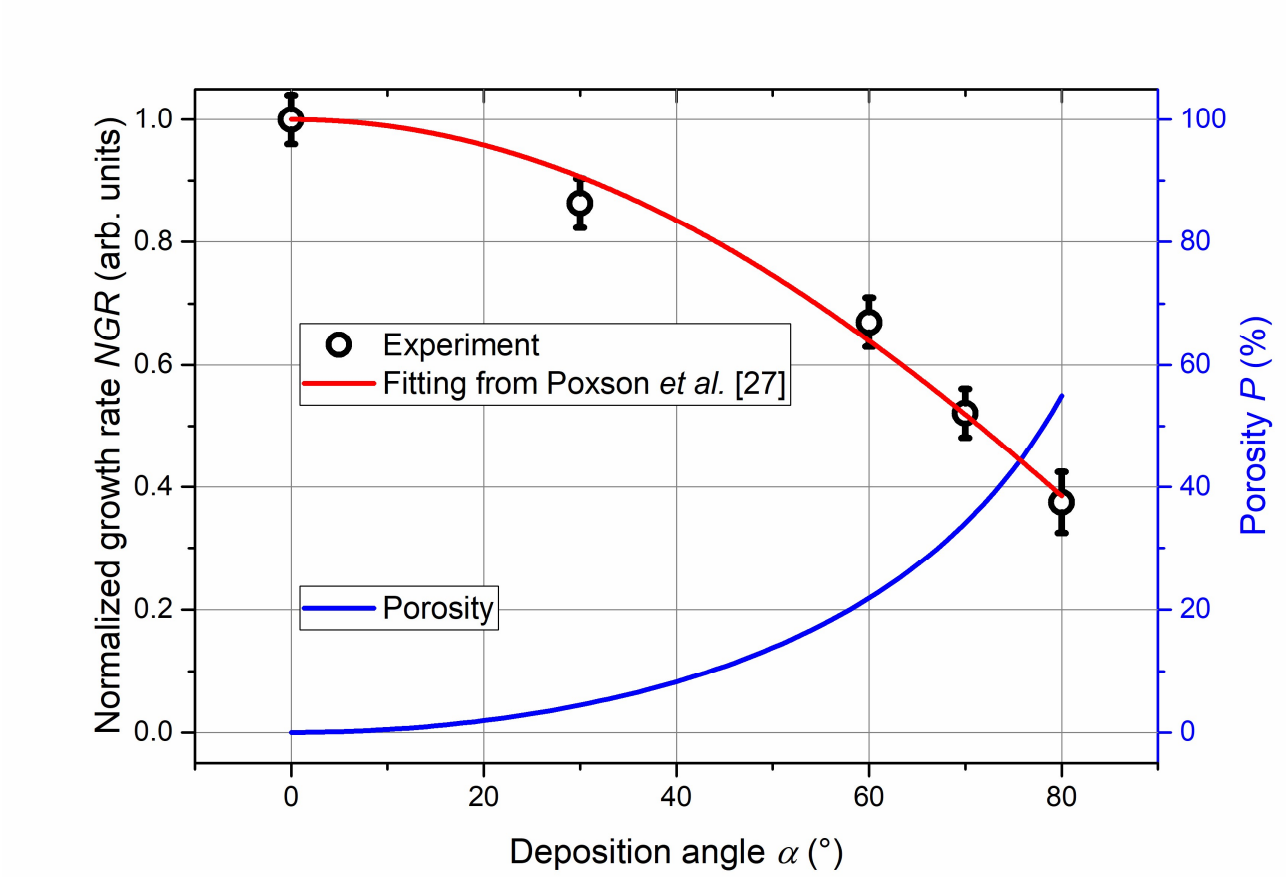

Figure 1: Normalized growth rate *NGR* as a function of the deposition angle α of sputter-deposited Au films. Symbols come from experiments and red line is a fitting obtained from Poxson's equation [27]. Porosity *P vs.* deposition angle α is also calculated (solid blue line) from fitting parameter based-on *NGR vs.* α evolution.

Fitting parameter c = 6.47 obtained from equation (1) is higher than that obtained for oxide materials prepared by evaporation [27]. This shows again that thermalization phenomenon of

sputtered particles has to be taken into account in OAD by sputtering compared to the evaporation process. In addition, equation (2) shows that *c* depends on the volume and height of a nanocolumn, and the cross-sectional area due to the shadowing created by the nanocolumn. In other words, the *c* parameter is to some extent, the result of atoms impinging on the column apex (*i.e.*, incident vapor flux) and adatom surface diffusion. For the gold material, surface diffusion energy is low compared to other transition metals like W or Mo [32]. Length of diffusion of Au adatoms allows the growth of columns with high column angles β. As a result, the height of the columns has to be significant enough before the shadowing effect becomes effective, which correlates with a low *c* parameter.

Porosity *P vs.* deposition angle α can also be calculated assuming the *c* parameter using [27]:

$$P = \frac{\alpha \tan \alpha}{c + \alpha \tan \alpha} \quad (3)$$

It is firstly interesting to note the reverse evolution of *NGR* and porosity *P* as a function of α, which is typical of AOD thin films. If a correct determination of the voided ratio in these films still remains a challenging task, the increase of the porosity as deposition angle rises has ever been reported, especially for transparent materials where refractive index gives an indirect but rather precise value of the overall film porosity [33]. As α is increased, the shadow length is favored, thereby preventing film deposition over a larger fraction of the substrate. Increasing the shadowing effect, the intercolumn void region expands, creating more spaces between columns and correspondingly reducing the density of the film. The shadow length is less than a few times the height of the surface feature up to deposition angles lower than around 70°. Such a length rises rapidly for α > 70° and becomes very long when forthcoming to glancing deposition angles (*i.e.*, α tending to 90°). For glancing conditions, the shadow length can greatly exceed the surface diffusion length and ballistic shadowing effect is the key parameter of the film growth. For our Au films prepared with a deposition angle α = 80°, the calculated porosity P reaches 55%, which is realistic enough when observing top and cross-section views by SEM (Fig. 2).

Au films prepared with a normal deposition angle (α = 0°) exhibit a quite dense morphology (fracture is not very well defined due to plastic behavior of gold) with a granular and poorly defined surface (Fig. 2a and 2e), as commonly observed for this sputter-deposited noble metal [34].

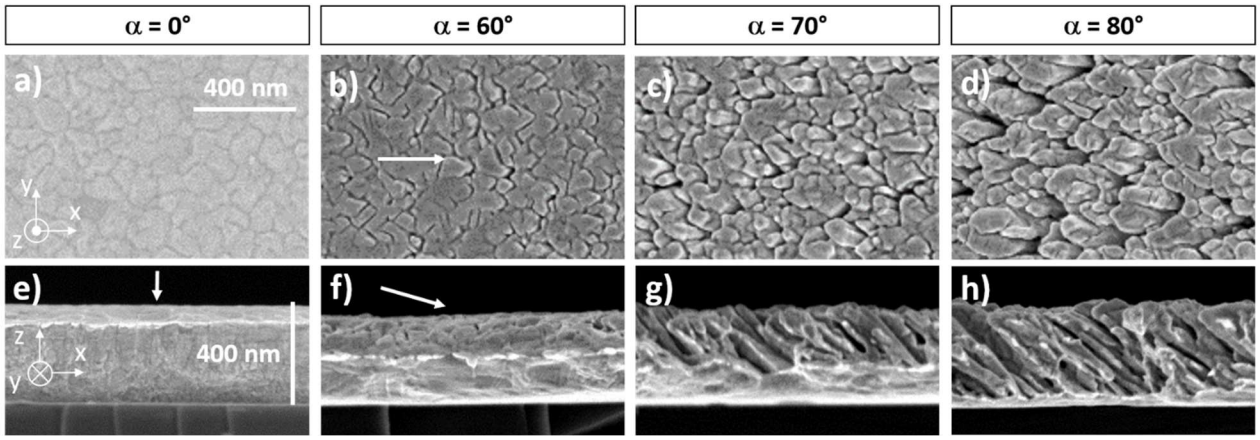

Figure 2: Top (a-d) and cross-section views (e-h) by SEM of Au thin films sputter-deposited at different deposition angles. White arrows indicate the direction of the incoming particle flux for α = 60° and for the other angles. For all pictures, the scale bar is the same.

Very similar film features are obtained for the lowest deposition angles (not shown here). When α is set to 60°, coalescence between grains is not so strong and boundaries between grains become more noticeable with a random distribution and a grain size around 100 nm (Fig. 2b). The cross-section is again unclearly defined although the film/air interface shows a granular surface morphology. Depositing with α = 70° gives rise to a clear tilted columnar architecture (column angle β = 42°), where the film cross-section is not entirely and frankly fractured (Fig. 2g). Columns are oriented following the direction of the incoming particle flux (white arrow) and spaces between columns are bigger. For the highest deposition angle α = 80°, columns are better defined and films appear even more porous with a column angle β = 50°. Although only two deposition angles (α = 70 and 80°) allow an accurate measurement of the column angle from SEM pictures, evolution of β *vs.* α does not correspond to empirical laws such as the tangent [35] or cosine [36] rule (Fig. S1 in Supplementary Material). Such laws are rather suitable for low deposition angles and sputtering

pressures involving ballistic particles mainly. For our operating conditions, β *vs.* α rather correlates with an enhanced relationship suggested by Lichter and Chen [37] where adatom surface diffusion, deposition rate and shadow feature height, are merged in a fitting parameter (Fig. S1 in Supplementary Material) without distinguishing the contribution coming from each phenomenon.

It is also worth of noting that the fanning effect can appear in the OAD columnar growth. It corresponds to a widening of the column cross-section in the direction perpendicular to the particle flux. Zhu *et al.* correlated this fanning effect with the melting point of the deposited metal [38]. For the gold material, one can assume that the surface diffusion of incoming atoms predominates. This reduces the lateral growth, hinders the fan structure and consequently does not favor the fan angle. Columns with isotropic cross-sections are rather produced but with connections to each other's, particularly in the direction perpendicular to the incoming particle flux.

Fig. 3 shows GIXRD patterns recorded for Au thin films 400 nm thick sputter-deposited on (100) Si wafer, and for different deposition angles α = 0° to 80°. For Au films prepared by conventional sputtering (α = 0°), a diffracted signal is mainly obtained at 2θ = 64.75° corresponding to the 220 Bragg reflection, whereas smaller peaks are measured at lower angles assigned to (111) and (200) planes. This highly intense diffraction of the (220) planes (associated with a low signal due to (111) planes) has ever been reported for vacuum-deposited gold films [39]. It is well known that several face-centered-cubic (fcc) metals like Al, Ag or Cu, naturally crystallize with a (111) texture. However, the type of substrate may interfere (especially (100) Si due to its cubic symmetry) with this natural tendency and inhibits the (111) growth. This 220 reflection becomes even more intense for Au films prepared with a deposition angle α of 30°. This increase of some diffracted peaks for similar ranges of α has also been noticed for other fcc metals like Cu where a maximum of intensity has even been measured [40]. This crystallinity improvement can be assigned to an enhancement of adatom mobility as the deposition angle rises. Inclining the substrate with an angle of a few tens degrees favors the diffusion of atoms impinging on the column apex, without prevailing the shadowing effect.

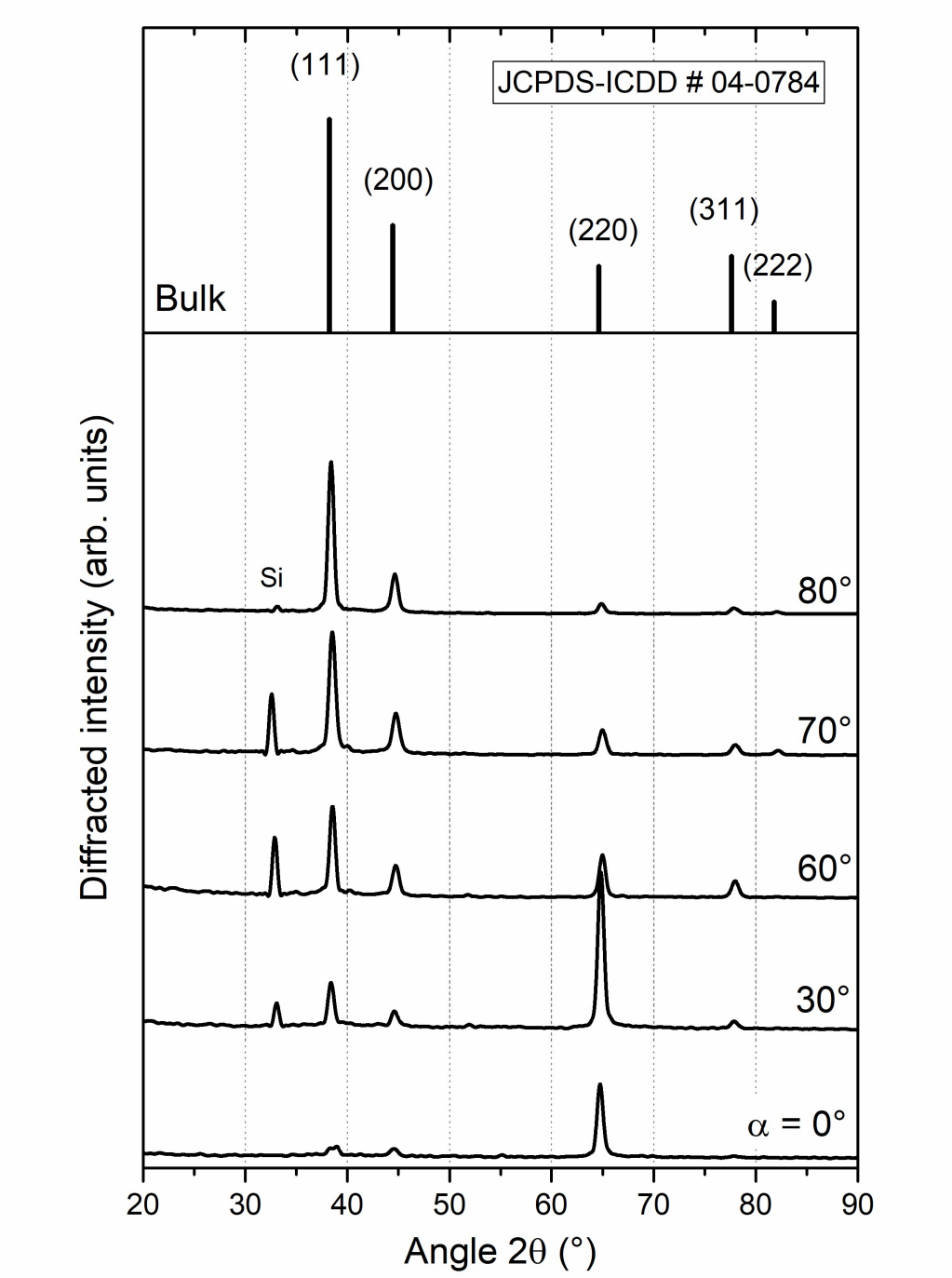

Figure 3: GIXRD patterns of Au bulk material and Au thin films 400 nm thick prepared on (100) Si substrate and for different deposition angles α = 0° to 80°.

A further increase of the deposition angle gives rise to a reverse evolution of peaks related to (111) and (220) planes, particularly when α is over than 60°. Such a value has ever been noticed as a critical angle for deposition of other metallic systems [41]. It is firstly assumed as the angle from

which the shadowing effect predominates and thus, influences the final morphology of deposited thin films. In addition, this range of angles has an influence on the crystalline structure of the columns since adatom mobility as well as lateral growth become significant parameters on the columnar growth.

GIXRD pattern recorded for $\alpha = 80°$ exhibits peaks very similar to those obtained with bulk material (JCPDS-ICDD #0 4-0784), as shown in Fig. 3. For this glancing angle of deposition, the columnar growth strongly depends on the surface diffusion of Au atoms occurring on the top of the columns. As a result, no preferred orientation is expected but rather a random growth. For all samples, the crystal size has been calculated from the Scherrer's law and assuming peaks due to (220), (200) and (111) planes (not shown here). Crystal size is in between 15-20 nm whatever the deposition angle and no clear trend has been noticed as a function of the deposition angle. It is also worth of remarking that intensity of diffracted signals evidently depends on the orientation of the OAD thin films towards the X-ray source, and thus deeper structural analyses of texture via pole figures should be interesting to perform. These investigations remain out of the scope of the paper and would require further analyses. However, and as previously noticed, when the deposition angle increases, Au thin films tend to growth as the gold polycrystalline material and so, one can wonder about electrical behaviors *vs.* temperature of the films.

3.2 Electrical resistivity vs. temperature

DC electrical resistivity ρ *vs.* temperature T was methodically measured from 7 to 300 K for all Au films (thickness = 400 nm) sputter-deposited on glass with a deposition angle α changing from 0° to 80°. A typical metallic-like behavior is systematically obtained, as illustrated in Fig. 4. A linear evolution is observed from ρ *vs.* T measurements for temperatures higher than a few tens of K. For this range of temperatures, the linear variation is usually observed in nonmagnetic metallic crystalline materials. Such a temperature dependence of the electrical resistivity is due to the electron-

phonon interactions. Decreasing the temperature and typically when it is lower than about 20 K, the film resistivity becomes independent on the temperature. This behavior defines the residual resistivity, which will be taken at 7 K, namely ρ_{7K}. This residual resistivity is related to electron scattering by defects (or impurities).

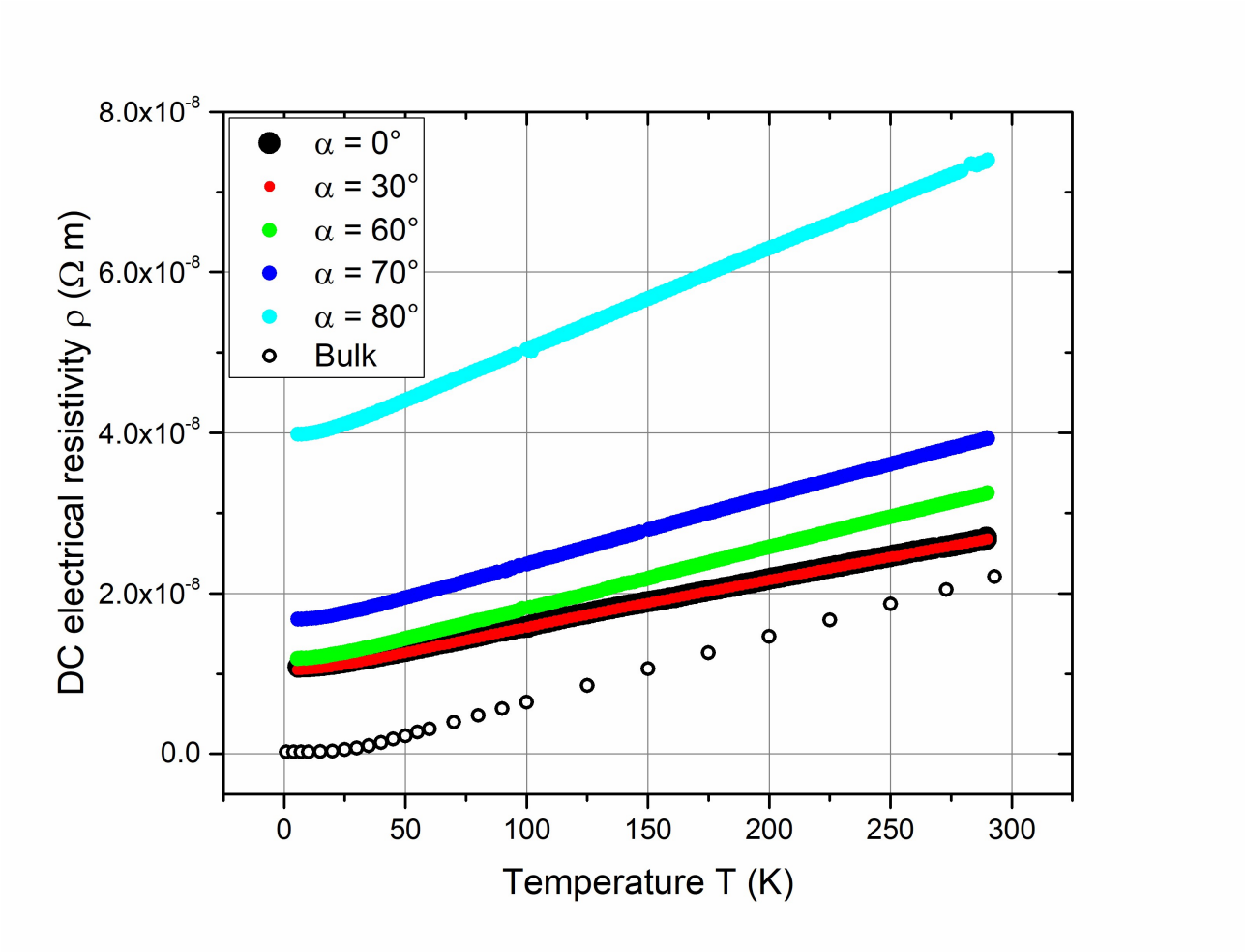

Figure 4: DC electrical resistivity ρ as a function of the temperature T of 400 nm thick Au thin films sputter-deposited on glass, and for 5 deposition angles α changing from 0° to 80°. The ρ *vs.* T evolution of Au bulk material is also shown.

As classically reported for metallic thin films and for all Au films, resistivity is higher than that of the bulk material, whatever the temperature. Because of the polycrystalline structure of Au films, the mean free path of electrons is lower than in the bulk, which favors scattering of the

electrons by grain boundaries and defects. For conventional sputtering (α = 0°) and deposition angle α =30°, ρ *vs. T* measurements exhibit nearly the same evolution. Since morphology and crystalline structure are very similar as previously noticed from SEM observations and GIXRD patterns, one can expect no significant differences of electronic transport behaviors for low deposition angles. As α rises, Au films become more resistive with the highest resistivity at 300 K over 7.10^{-8} Ω m for films prepared with a deposition angle of 80°. This increase of resistivity has often been reported for other metals sputter-deposited by OAD [16-21]. When deposition angle increases, the growth of tilted columns develops bigger voids and for some metals, smaller crystal size [26] leading to an enhanced scattering of electrons, a decrease of their mean free path and so a more resistive medium. For our Au films, since no changes of the crystal size has been observed as a function of the deposition angle (previously stated from XRD analyses), changes of resistivity are mainly assigned to the voided columnar structure. It is also interesting of noticing that this increase of resistivity is particularly marked when α > 60°, which again correlates with the critical angle previously observed from analyses of the morphology by SEM (Fig. 2) and crystalline structure by GIXRD (Fig. 3).

In order to understand electronic transport properties in Au OAD thin films, the electron-phonon and electron-defect interactions are assumed based-on the temperature-dependence electrical resistivity. The latter is obtained from the addition of two contributions. The first one is the residual resistivity ρ_0 caused by electron scattering by grain boundaries, static impurities and defects, which is mainly temperature-independent, and taken at 7 K in our study (i.e., ρ_{7K}). The second one is the intrinsic resistivity related to thermal vibrations of the lattice (phonons) and shows a temperature dependent behavior. In simple metals such as noble metals, the electrical resistivity ρ as a function of the temperature *T* is well described by the following Bloch-Grüneisen formula:

$$\rho = \rho_0 + A\left(\frac{T}{\theta_D}\right)^n \int_0^{\frac{\theta_D}{T}} \frac{x^n dx}{(e^x-1)(1-e^{-x})} \quad (4)$$

where $\rho_0 = \rho_{7K}$ is the residual resistivity taken at 7 K (Ω m), *A* the electron-phonon coupling constant (Ω m), θ_D the Debye temperature (K), and *n* an exponent depending on the dominant scattering

mechanism. For a dominant electron-electron scattering mechanism $n = 2$, n = 3 corresponds to s-d electron scattering, $n = 4.5$ to electron-magnon scattering, and $n = 5$ to electron-acoustic phonon scattering. Several scattering mechanisms may occur at the same time and for the same range of temperatures. However, the $n = 5$ value has been assumed for our Au films as commonly reported for this kind of noble metal since the temperature variation of resistivity is known to be of T^5 kind (electron-acoustic phonon scattering mechanism predominates) [42] since Au is nonmagnetic material.

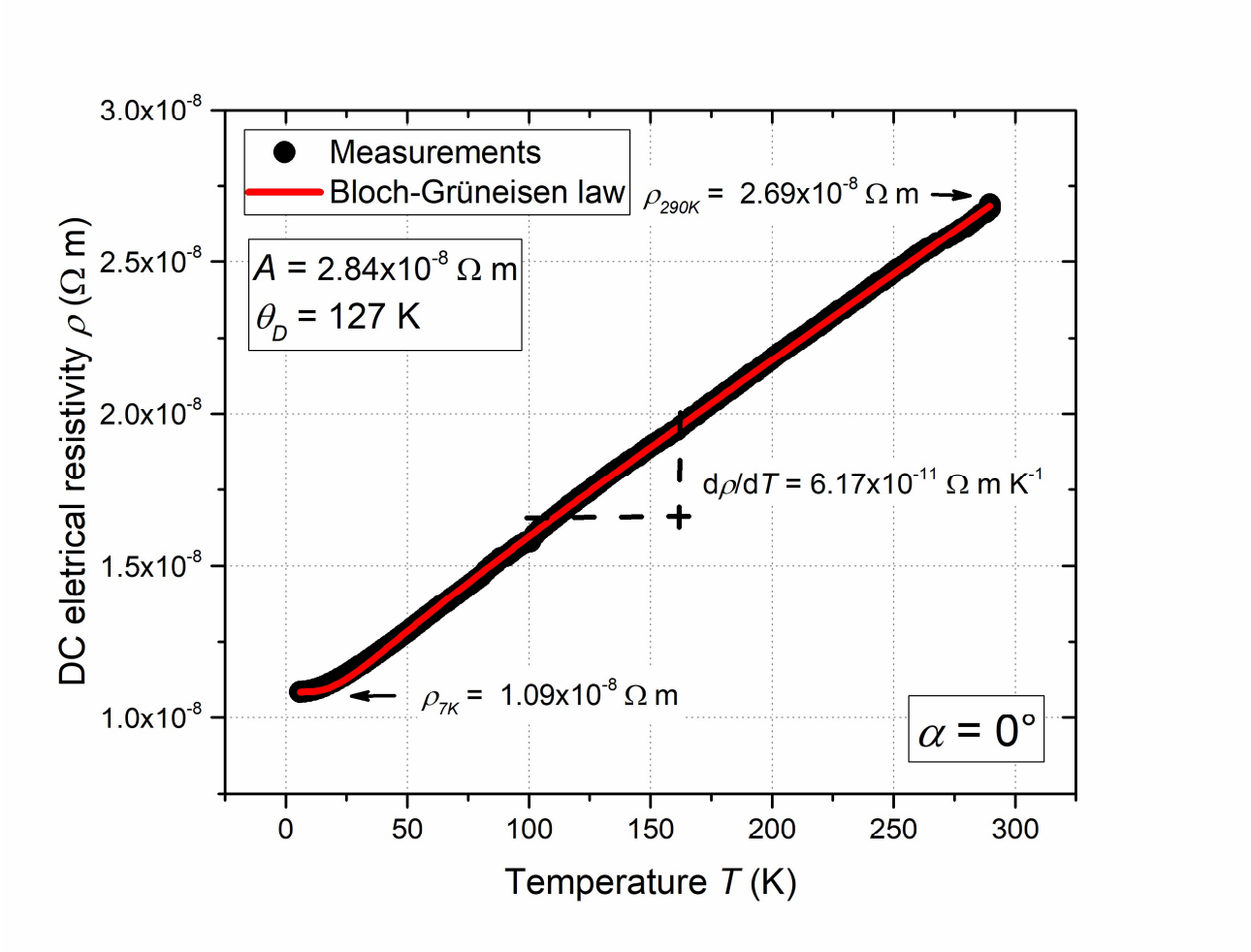

Figure 5: An example of experimental measurements and fitting assuming the Bloch-Grüneisen formula (equation (4)) obtained for DC electrical resistivity ρ *vs.* temperature T of 400 nm thick Au thin films sputter-deposited on glass by conventional process (*i.e.*, $\alpha = 0°$). For all studied deposition angles, measurements and fittings of ρ *vs.* T are shown in section III of Supplementary Material.

For all films, the measured resistivity data ρ *vs.* T have been fitted using equation (4) and running a home-made Python program (to see Section II of Supplementary Material). The A and θ_D parameters have been taken as adjustable coefficient for fitting in the entire temperature range 7-300 K, as illustrated in Fig. 4 for Au films prepared with a deposition angle $\alpha = 0°$. Fitting results are all shown in Section III of Supplementary Material. For the example given in Fig. 4, it gives rise to $A = 2.84\times10^{-8}$ Ω m and $\theta_D = 127$ K. These values are significantly different to those of Au bulk material ($A = 5.59\times10^{-8}$ Ω m and $\theta_D = 185$ K from Table 1).

α (°)	0	30	60	70	80	Bulk
ρ_{300K} (Ω m)	2.69×10^{-8}	2.68×10^{-8}	3.25×10^{-8}	3.97×10^{-8}	7.38×10^{-8}	2.27×10^{-8}
ρ_{7K} (Ω m)	1.09×10^{-8}	1.05×10^{-8}	1.19×10^{-8}	1.67×10^{-8}	3.98×10^{-8}	2.21×10^{-10}
RRR	2.47	2.55	2.73	2.38	185	103
$d\rho/dT$ (Ω m K^{-1})	6.17×10^{-11}	6.21×10^{-11}	7.54×10^{-11}	8.45×10^{-11}	1.29×10^{-10}	8.58×10^{-11}
TCR_{300K} (K^{-1})	2.29×10^{-3}	2.32×10^{-3}	2.32×10^{-3}	2.13×10^{-3}	1.75×10^{-3}	3.78×10^{-3}
A (Ω m)	2.84×10^{-8}	2.65×10^{-8}	4.21×10^{-8}	4.42×10^{-8}	6.42×10^{-8}	5.59×10^{-8}
θ_D (K)	127	117	147	140	135	185

Table 1: Main characteristics of DC electrical resistivity and fitting parameters obtained from equation (2) for Au thin films prepared with different deposition angles α. ρ_{300K} is the DC electrical resistivity at 300 K (Ω m); ρ_{7K} is the DC electrical resistivity at 7 K (Ω m); *RRR* is the residual resistivity ratio (ρ_{300K}/ρ_{7K}); $d\rho/dT$ is the temperature derivative of DC electrical resistivity (Ω m K^{-1}); *TCR* is the temperature coefficient of resistance obtained at 300 K ($1/\rho_{300K}\times(d\rho/dT)_{300K}$); A and θ_D are a fitting coefficient (prefactor in Ω m) and the Debye temperature (K) obtained from fitting assuming equation (4), respectively.

Such deviations between thin films and bulk materials of electron-phonon coupling constant and Debye temperature have ever been reported by others and for various metals prepared by conventional deposition processes [43-45]. Softening of phonons is the mechanism particularly put forward to explain these discrepancies [46-48]. As α changes from 0° to 80°, electron-phonon coupling constant and Debye temperature both tend to increase and reach $A = 6.42\times10^{-8}$ Ω m and θ_D = 135 K for the highest deposition angle, respectively. This means that softening of phonons reduces for Au films prepared with the highest deposition angles. Based-on Yeh *et al.* investigations [49], the electron-phonon scattering rate depends on the longitudinal-to-transverse phonons ratio. Although the porous structure is favored with a rising deposition angle, crystal size does not significantly change as a function of the deposition angle (15 to 20 nm from XRD patterns in Fig. 3). A polycrystalline structure is favored, which correlates with the trend of the electron-phonon coupling constant and the Debye temperature to behave like the bulk gold material, and so electron scattering is dominated by interaction with longitudinal rather than transverse phonons in Au OAD thin films.

These A and θ_D values calculated from our fitting procedure are also corroborated with the experimental evolution of $d\rho/dT$ *vs.* α, as reported in Table 1. The slope $d\rho/dT$ (calculated for our samples at 100 K) is directly related to electron-phonon interactions and is used as a measure of the coupling constant [50]. This also means that Au OAD films prepared with the highest glancing angles are more sensitive to the temperature, and their electronic transport properties become even more dominated by the electron-phonon interactions. However, compared to other transition metals and assuming the values obtained for Au bulk material (Table 1), $d\rho/dT$ of our films are lower than the MIR (Mott-Ioffe-Regel) limit as stated for OAD simple metals [26] and conventional metallic thin films (around 10^{-8} Ω m K^{-1} from [51]). This is mainly assigned to the nearly constant crystal size of 15-20 nm even though the deposition angle rises (which does not disturb the electron scattering at grain boundaries). As a result, Au OAD films prepared with a growing deposition angle α from 0° to

80° cannot be described as “bad metals” like it was previously shown for other single metallic films, especially for the most glancing deposition angles [26]. Although $d\rho/dT$ significantly increases as a function of the residual resistivity obtained at 7 K (ρ_{7K}), it still remains well below the MIR limit and can be rather considered as “good metals”. It is also worth of noting that the residual resistivity ratio ($RRR = \rho_{300K}/\rho_{7K}$) as well as the temperature coefficient of resistance at 300 K ($TCR_{300K} = 1/\rho_{300K}\times(d\rho/dT)_{300K}$) both increase as a function of the deposition angle α (Table 1). This means that the electron-phonon interactions prevail on the increase of resistivity due to voids between the polycrystalline tilted columns leading to a high temperature coefficient of resistance. In addition, as similarly reported in other AOD thin films [25, 26, 52], depositing with a glancing angle induces structural defects at the atomic scale favoring the electron-defects scattering phenomenon at low temperature and thus a high residual resistivity ratio.

4. Conclusions

Gold thin films 400 nm thick were deposited by DC magnetron sputtering using the oblique angle deposition (OAD) process. The deposition angle α was gradually and methodically changed from 0° to 80°. For the lowest angles and up to α = 60°, films exhibit a dense microstructure and coalescent grains with a strong preferential orientation along the (220) crystallographic planes. For deposition angles α > 60°, the shadowing effect starts acting significantly and a tilted columnar structure appears. Clear voids between columns are produced and these tilted columns are made of polycrystalline grains with no substantial evolution of the crystal size as α rises and they remain in-between 15-20 nm whatever the deposition angle.

Similarly, the electronic transport properties were instigated at low temperature from DC electrical resistivity ρ *vs.* temperature T measurements in the range 7-300 K. These ρ *vs.* T measurements showed a typical metallic-like behavior for all films and whatever the deposition angle. Electrical resistivity strongly increases as the deposition angle changes from 0° to 80°. Again, the

deposition angle has to reach 60° to produce some major modifications of the film resistivity. The Bloch-Grüneisen law was successfully used to accurately fit ρ *vs.* T measured data for all Au OAD thin films. Debye temperature as well as the electron-phonon coupling constant both increased and tended to values of the bulk Au material for the highest deposition angles. These results were correlated with the crystallographic structure showing a better polycrystalline feature with high structural defects of the tilted columns when the deposition angle reached 80°. This study illustrates how the architecture of Au OAD thin films can influence electron-phonon interactions. This electron scattering remains predominant in spite of the increase of resistivity, the latter being assigned to the voids between the polycrystalline tilted columns as the deposition angle tends to the most glancing angles.

CRediT authorship contribution statement

Nicolas Martin: Writing - review & editing; Supervision; Funding acquisition. **Eliot Martin:** Software; Validation; Writing - review & editing. **Jean-Marc Cote:** Data curation; Software; Validation; Writing - review & editing. **Fabrice Sthal:** Validation; Writing - review & editing. **Joseph Gavoille:** Data curation; Validation; Writing - review & editing. **Marina Raschetti:** Data curation; Validation; Software; Writing - review & editing. **Stefania Oliveri:** Data curation; Validation; Writing - review & editing.

All authors have read and agreed to the published version of the manuscript.

Declaration of Competing Interest

The authors declare that they have no known competing financial interests or personal relationships that could have appeared to influence the work reported in this paper.

Data availability

Data will be made available on request.

Acknowledgements

This work has been achieved in the frame of the EIPHI Graduate school (contract "ANR-17-EURE-0002" and by the Bourgogne-Franche-Comté Region. It has also been partly supported by the French RENATECH network and its FEMTO-ST technological facility.

Appendix A: Supplementary data

Supplementary Material to this article can be found on line at https:// …

References

[1] B. Feldman, R. Deng, S.T. Dunham, Dependence of resistivity on surface profile in nanoscale metal films and wires, J. Appl. Phys., 103 (2008) 113715-4, https://doi.org/10.1063/1.2937085.

[2] J.W.C. De Vries, Temperature and thickness dependence of the resistivity of thin polycrystalline aluminium, cobalt, nickel, palladium, silver and gold films, Thin Solid Films, 167 (1988) 25-32, https://doi.org/10.1016/0040-6090(88)90478-6.

[3] C. Adelman, On the extraction of resistivity and area of nanoscale interconnect lines by temperature-dependent resistance measurements, Solid State Electron., 152 (2019) 72-80, https://doi.org/10.1016/j.sse.2018.12.005.

[4] R.C. Munoz, G. Vidal, M. Mulsow, J.G. Lisoni, C. Arenas, A. Concha, F. Mora, R. Espejo, Surface roughness and surface-induced resistivity of gold films on mica: Application of quantitative scanning tunneling microscopy, Phys. Rev. B, 62 (2000) 4686-4697, https://doi.org/10.1103/physrevb.62.4686.

[5] D.K. Sharma, R. Srivastava, Negative temperature coefficient of resistivity in thin metallic wires, J. Mater. Sci. Lett. 2 (1983) 775-776, https://doi.org/10.1007/bf00720557.

[6] H.D. Wang, J.H. Liu, X. Zhang, Z.Y. Guo, K. Takahashi, Experimental study on the influences of grain boundary scattering on the charge and heat transport in gold and platinum nanofilms, Heat Mass Transf 47 (2011) 893-898, https://doi.org/10.1007/s00231-011-0825-5.

[7] T. Sun, B. Yao, A.P. Warren, K. Barmak, M.F. Toney, R.E. Peale, K.R. Coffey, Dominant role of grain boundary scattering in the resistivity of nanometric Cu films, Phys. Rev. B 79 (2009) 0414402-0414404, https://doi.org/10.1103/physrevb.79.041402.

[8] A.L. Lima, X. Zhang, A. Misra, C.H. Booth, E.D. Bauer, M.F. Hundley, Length scale effects on the electronic transport properties of nanometric Cu/Nb multilayers, Thin Solid Films 515 (2007) 3574-3579, https://doi.org/10.1016/j.tsf.2006.11.004.

[9] A. Barranco, A. Borras, A.R. Gonzalez-Elipe, A. Palmero, Perspectives on oblique angle deposition of thin films: from fundamentals to devices, Progr. Mater. Sci. 76 (2016) 59-153, https://doi.org/10.1016/j.pmatsci.2015.06.003.

[10] D.X. Ye, T. Karabacak, R.C. Picu, G.C. Wang, T.M. Lu, Uniform Si nanostructures grown by oblique angle deposition with substrate swing rotation, Nanotechnology, 16 (2005) 1717-1723, https://doi.org/10.1088/0957-4484/16/9/052.

[11] M.M. Hawkeye, M.T. Taschuk, M.J. Brett, Glancing Angle Deposition of Thin Films: Engineering the Nanoscale, John Wiley & Son Ltd, Chichester, 2014, https://doi.org/10.1002/9781118847510.

[12] A. Yildiz, H. Cansizoglu, T. Karabacak, Electrical transport in AZO nanorods, Appl. Surf. Sci., 352 (2015) 2-4, https://doi.org/10.1016/j.apsusc.2015.02.067.

[13] F. Chaffar Akkari, H. Ben Jbara, D. Abdelkader, B. Gallas, M. Kanzari, Effect of angle deposition γ on the structural, optical and electrical properties of copper oxide zigzag (+γ, −γ) nanostructures elaborated by glancing angle deposition, Thin Solid Films, 657 (2018) 61-69, https://doi.org/10.1016/j.tsf.2018.05.006.

[14] S. Morikawa, Y. Satake, M. Takashiri, Characteristics of nanostructured bismuth telluride thin films fabricated by oblique deposition, Vacuum, 148 (2018) 296-302, https://doi.org/10.1016/j.vacuum.2017.11.035.

[15] M.S. Rodrigues, P. Fiedler, N. Küchler, R.P. Domingues, C. Lopes, J. Borges, J. Haueisen, F. Vaz, Dry electrodes for surface electromyography based on architectured Titanium thin films, Materials, 13 (2020) 2135-13, https://doi.org/10.3390/ma13092135.

[16] R. El Beainou, J.M. Cote, V. Tissot, V. Potin, N. Martin, Resistivity anisotropy of tilted columnar W and W-Cu thin films, Surf. Coat. Technol., 421 (2021) 127412-11, https://doi.org/10.1016/j.surfcoat.2021.127412.

[17] C. Lopes, M.S. Rodrigues, A. Ferreira, F. Macedo, I. Borsan, C. Gabor, M.A. Pop, E. Alves, N.P. Barradas, D. Munteanu, F. Vaz, The influence of the nanostructure design on the optical, electrical and thermal properties of TiN_x thin films prepared by reactive magnetron sputtering, Mater. Chem. Phys. 306 (2023) 127981-19, https://doi.org/10.1016/j.matchemphys.2023.127981.

[18] J. Potočnik, N. Božinović, M. Popović, T. Barudžija, M. Nenadović, M. Novaković, Fabrication of zigzag and square spiral Cu nanostructures: Influence of substrate rotation on the structural, optical and electrical properties J. Alloy. Compd., 922 (2022) 166211-9, https://doi.org/10.1016/j.jallcom.2022.166211.

[19] A. Besnard, N. Martin, L. Carpentier, B. Gallas, A theoretical model for the electrical properties of chromium thin films sputter deposited at oblique incidence, J. Phys. D: Appl. Phys., 44 (2011) 215301-8, https://doi.org/10.1088/0022-3727/44/21/215301.

[20] A. Ferreira, P. Pedrosa, N. Martin, M. Arab Pour Yazdi, A. Billard, S. Lanceros-Méndez, F. Vaz, Nanostructured $Ti_{1-x}Cu_x$ thin films with tailored electrical and morphological anisotropy, Thin Solid Films, 672 (2019) 47-54, https://doi.org/10.1016/j.tsf.2019.01.008.

[21] S. Oliveri, J.M. Cote, M. Raschetti, P. Roux, N. Martin, Glancing angle deposition for tuning electronic transport properties of Si thin films, Phys. Lett. A, 480 (2023) 128955-3, https://doi.org/10.1016/j.physleta.2023.128955.

[22] J.A. Khan, Y. Maithani, J.P. Singh, Ag_2Se nanorod arrays with ultrahigh room temperature Thermoelectric Performance and superior mechanical properties, ACS Appl. Mater. Interfaces, 15(29) (2023) 35001-35013, https://doi.org/10.1021/acsami.3c06231.s001.

[23] V. Collado, N. Martin, P. Pedrosa, J.Y. Rauch, M. Horakova, M. Arab Pour Yazdi, A. Billard, Temperature dependence of electrical resistivity in oxidized vanadium films grown by the GLAD technique, Surf. Coat. Technol., 304 (2016) 476-485, https://doi.org/10.1016/j.surfcoat.2016.07.057.

[24] A. Besnard, N. Martin, F. Sthal, L. Carpentier, J.Y. Rauch, Metallic to dielectric transition in titanium GLAD thin films sputter deposited, Funct. Mater. Lett., 6 (2013) 1250051-5, https://doi.org/10.1142/S1793604712500518.

[25] Z. Ali, D. Basaula, W. Zhou, J. Brock, M. Khan, K.F. Eid, Controlling the charge transport mode in permalloy films using oblique angle deposition, J. Magn. Magn. Mater., 484 (2019) 430-436, https://doi.org/10.1016/j.jmmm.2019.03.087.

[26] H. Gerami, J.M. Cote, A.J. Santos, N. Martin, Low temperature dependence of electrical resistivity in obliquely sputter-deposited transition metal thin films, Surf. Interfaces, 54 (2024) 105113-11, https://doi.org/10.1016/j.surfin.2024.105113.

[27] D.J. Poxson, F.W. Mont, M.F. Schubert, J.K. Kim, E.F. Schubert, Quantification of porosity and deposition rate of nanoporous films grown by oblique-angle deposition, Appl. Phys. Lett. 93 (2008) 101914-3, https://doi.org/10.1063/1.2981690.

[28] Z.J. Radzimski, W.M. Posadowski, S.M. Rossnagel, S. Shingubara Directional copper deposition using dc magnetron self-sputtering, J. Vac. Sci. Technol., B16(3) (1998) 1102-1106, https://doi.org/10.1116/1.590016.

[29] Q. Zhou, Z. Li, J. Ni, Z. Zhang, A Simple Model to Describe the Rule of Glancing Angle Deposition, Mater. Trans., 52(3) (2011) 469-473, https://doi.org/10.2320/matertrans.m2010342.

[30] V. Potin, H. Boukhalfa, N. Martin, Oblique angle co-deposition of nanocolumnar tungsten thin films with two W sources: Effect of pressure and target current, Mater. Chem. Phys., 281 (2022) 125864-11, https://doi.org/10.1016/j.vacuum.2022.111347.

[31] R. Alvarez, J.M. Garcia-Martin, M.C. Lopez-Santos, V. Rico, F.J. Ferrer, J. Cotrino, A.R. Gonzalez-Elipe, A. Palmero, On the deposition rates of magnetron sputtered thin films at oblique angles, Plasma Process. Polym. 11 (6) (2014) 571–576, https://doi.org/10.1002/ppap.201300201.

[32] S.Y. Davydov, Calculation of the activation energy for surface self-diffusion of transition metal atoms, Phys. Solid State, 41(1) (1999) 8-10, https://doi.org/10.1134/1.1130717.

[33] S.H. Woo, Y.J. Park, D.H. Chang, K.M.A. Sobahan, C.K. Hwangbo, Wideband antireflection coatings of porous MgF_2 films by using glancing angle deposition, J. Korean Phys. Soc., 51(4) (2007) 1501-1506, https://doi.org/10.3938/jkps.51.1501.

[34] F. Ruffino, V. Torrisi, G. Marleta, M.G. Grimaldi, Growth morphology of nanoscale sputter-deposited Au films on amorphous soft polymeric substrates, Appl. Phys. A, 103 (2011) 939-949, https://doi.org/10.1007/s00339-011-6413-1.

[35] J.M. Nieuwenhuizen, H.B. Haanstra, Microfractography of thin films, Philips Tech. Rev., 27 (1966) 87-91.

[36] R.N. Tait, T. Smy, M.J. Brett, Modelling and characterization of columnar growth in evaporated films, Thin Solid Films, 226 (1993) 196-201, https://doi.org/10.1016/0040-6090(93)90378-3.

[37] S. Lichter, J. Chen, Model for columnar microstructure in thin solid films, Phys. Rev. Lett., 56 (1986) 1396-1399, https://doi.org/10.1103/physrevlett.56.1396.

[38] H. Zhu, W. Cao, G.K. Larsen, R. Toole, Y. Zhao, Tilting angle of nanocolumnar films fabricated by oblique angle deposition, J. Vac. Sci. Technol. B30(3) (2012) 030606-4, https://doi.org/10.1116/1.4710999.

[39] Y. Golan, L. Margulis, I. Rubinstein, Vacuum-deposited gold films, Surf. Sci., 264 (1992) 312-326, https://doi.org/10.1016/0039-6028(92)90188-c.

[40] F. Chaffar Akkari, M. Kanzari, B. Rezig, Preparation and characterization of obliquely deposited copper oxide thin films, Eur. Phys. J. Appl. Phys., 40 (2007) 49-54, https://doi.org/10.1051/epjap:2007128.

[41] A. Siad, A. Besnard, C. Nouveau, P. Jacquet, Critical angles in DC magnetron thin films, Vacuum, 131 (2016) 305-311, https://doi.org/10.1016/j.vacuum.2016.07.012.

[42] W. Ma, X. Zhang, K. Takahashi, Electrical properties and reduced Debye temperature of polycrystalline thin gold, J. Phys. D: Appl. Phys., 43 (2010) 465301-8, https://doi.org/10.1088/0022-3727/43/46/465301.

[43] J. Sambles, K.C. Elsom, D.J. Jarvis, The resistivity of thin gold films, Solid State Commun., 32 (1979) 997-1000, https://doi.org/10.1016/0038-1098(79)90814-7.

[44] D.G. Westlake, L.C.R. Alfred, Determination of the Debye characteristic temperature of vanadium from the Bloch-Grüneisen relation, J. Phys. Chem. Solids, 29 (1968) 1931-1934, https://doi.org/10.1016/0022-3697(68)90043-7.

{45] Y.P. Timalsina, A. Horning, R.F. Spivey, K.M. Lewis, T.S. Kuan, G.C. Wang, T.M. Lu, Effects of nanoscale surface roughness on the resistivity of ultrathin epitaxial copper, Nanotechnology, 26 (2015) 075704-10, https://doi.org/10.1088/0957-4484/26/7/075704.

[46] N N.G. Ptitsina, G.M. Chulkova, K.S. Il'in, A.V. Sergeev, F.S. Pochinkov, E.M. Gershenzon, M.E. Gershenzon, Electron-phonon interaction in disordered metal films: The resistivity and electron dephasing rate, Phys. Rev. B 56(16) (1997) 10089-10096, https://doi.org/10.1103/physrevb.56.10089.

[47] W. Ma, T. Miao, X. Zhang, Thermal and electronic transport characteristics of polycrystalline thin gold, Proceedings of the 14th International Heat Transfer Conference – IHTC14, 6 (2010) 337-334, https://doi.org/10.1115/ihtc14-22328.

[48] J. Joseph, C. Bansal, K.J. Reddy, A. Rajanikanth, Electron–electron interaction dominated resistivity minimum in quasi-continuous Ag nanocluster films, AIP Adv., 10, (2020) 125223-4, https://doi.org/10.1063/5.0033098.

[49] S.S. Yeh, J.J. Lin, J. Xiunian, Z. Dianlin, Electron-phonon-impurity interference effect in disordered $Au_{56}Pd_{44}$ and IrO_2 thick films, Phys. Rev. B 72 (2005) 024204-5, https://doi.org/10.1103/physrevb.72.024204.

[50] A. Bid, A. Bora, A.K. Raychaudhury, Temperature dependence of the resistance of metallic nanowires of diameter ≥ 15 nm: Applicability of Bloch-Grüneisen theorem, Phys. Rev. B, 74 (2006) 035426-9, https://doi.org/10.1103/physrevb.74.035426.

[51] Q. Guo, C. Magen, M.J. Rozenberg, B. Noheda, Phenomenological classification of metals based on resistivity, Phys. Rev. B, 106 (2022) 085141-6, https://doi.org/10.1103/physrevb.106.085141.

[52] Z. Ali, D. Basaula, K.F. Eid, M. Khan, Anisotropic properties of oblique angle deposited permalloy thin films, Thin Solid Films, 735 (2021) 138899-8, https://doi.org/10.1016/j.tsf.2021.138899.

Figure captions

Figure 1

Normalized growth rate *NGR* as a function of the deposition angle α of sputter-deposited Au films. Symbols come from experiments and red line is a fitting obtained from Poxson's equation [27]. Porosity *P vs.* deposition angle α is also calculated (solid blue line) from fitting parameter based-on *NGR* vs. α evolution.

Figure 2

Top (a-d) and cross-section views (e-h) by SEM of Au thin films sputter-deposited at different deposition angles. White arrows indicate the direction of the incoming particle flux for $\alpha = 60°$ and for the other angles. For all pictures, the scale bar is the same.

Figure 3

GIXRD patterns of Au bulk material and Au thin films 400 nm thick prepared on (100) Si substrate and for different deposition angles $\alpha = 0°$ to 80°.

Figure 4

DC electrical resistivity ρ as a function of the temperature *T* of 400 nm thick Au thin films sputter-deposited on glass, and for 5 deposition angles α changing from 0° to 80°. The ρ *vs. T* evolution of Au bulk material is also shown.

Figure 5

An example of experimental measurements and fitting assuming the Bloch-Grüneisen formula (equation (4)) obtained for DC electrical resistivity ρ *vs.* temperature *T* of 400 nm thick Au thin films

sputter-deposited on glass by conventional process (*i.e.*, $\alpha = 0°$). For all studied deposition angles, measurements and fittings of ρ *vs.* T are shown in section III of Supplementary Material.

Table captions

Table 1

Main characteristics of DC electrical resistivity and fitting parameters obtained from equation (2) for Au thin films prepared with different deposition angles α. ρ_{300K} is the DC electrical resistivity at 300 K (Ω m); ρ_{7K} is the DC electrical resistivity at 7 K (Ω m); *RRR* is the residual resistivity ratio (ρ_{300K}/ρ_{7K}); $d\rho/dT$ is the temperature derivative of DC electrical resistivity (Ω m K^{-1}); *TCR* is the temperature coefficient of resistance obtained at 300 K ($1/\rho_{300K}\times(d\rho/dT)_{300K}$); A and θ_D are a fitting coefficient (prefactor in Ω m) and the Debye temperature (K) obtained from fitting assuming equation (4), respectively.